Laboratory Experiments on Eddy Generation by a Buoyant Coastal Current Flowing over Variable Bathymetry*

CHRISTOPHER L. WOLFE

College of Oceanic and Atmospheric Sciences, Oregon State University, Corvallis, Oregon

CLAUDIA CENEDESE

Physical Oceanography Department, Woods Hole Oceanographic Institution, Woods Hole, Massachusetts

(Manuscript received 23 September 2004, in final form 20 April 2005)

ABSTRACT

Irminger rings are warm-core eddies formed off the west coast of Greenland. Recent studies suggest that these eddies, which are implicated in the rapid springtime restratification of the Labrador Sea, are formed by an internal instability of the West Greenland Current (WGC), triggered by bathymetric variations. This study seeks to explore the effect of the magnitude and downstream length scale of bathymetric variations on the stability of a simple model of the WGC in a series of laboratory experiments in which a buoyant coastal current was allowed to flow over bathymetry consisting of piecewise constant slopes of varying magnitude. The currents did not form eddies over gently sloping bathymetry and only formed eddies over steep bathymetry if the current width exceeded the width of the sloping bathymetry. Eddying currents were immediately stabilized if they flowed onto gently sloping topography. Bathymetric variations that persisted only a short distance downstream perturbed the flow locally but did not lead to eddy formation. Eddies formed only once the downstream length of the bathymetric variations exceeded a critical scale of about 8 Rossby radii. These results are consistent with the observed behavior of the WGC, which begins to form Irminger rings after entering a region where the continental slope abruptly steepens and becomes narrower than the WGC itself in a region spanning about 20–80 Rossby radii of downstream distance.

1. Introduction

The West Greenland Current (WGC) is a swift, buoyancy-driven current that flows poleward over the west Greenland shelf and slope. This current is composed of two different water masses originating on the east side of Greenland: a cold, fresh Arctic-origin component that is an extension of the East Greenland Current and a warm, salty Gulf Stream–origin component that can be seen as an extension of the Irminger Current (Sverdrup et al. 1942; Krauss 1986, 1995; Pickart et al. 2005; Fratantoni and Pickart 2005, manuscript submitted to *J. Phys. Oceanogr.*). The cold, fresher water is found predominantly over the continental shelf while the salty, warm water flows farther offshore, over the continental slope. Though these water masses are distinguishable by temperature and salinity, they are merged to form a single broad velocity and density core. Several authors have proposed alternate naming schemes that distinguish the two water masses [e.g., Katsman et al. (2004) refers to the warm, salty component as the "Irminger Current" and R. A. Clarke (2005, personal communication) prefers the name "West Greenland/Irminger current system"], but to avoid confusion we will continue to use the historical name.

The bathymetry of the Labrador Sea is shown in Fig. 1, along with schematic representations of the two components of the WGC. The west Greenland bathymetry shows a region (gray box in Fig. 1) where the 500–2500-m isobaths become close together, indicating a steepening of the bottom slope. We will refer to this region as the "gap" in which the bathymetry steepens when compared with the bathymetry before or after

* Woods Hole Oceanographic Institution Contribution Number 11230.

Corresponding author address: Christopher L. Wolfe, College of Oceanic and Atmospheric Sciences, Oregon State University, 104 COAS Admin. Bldg., Corvallis, OR 97331-5503.
E-mail: cwolfe@coas.oregonstate.edu

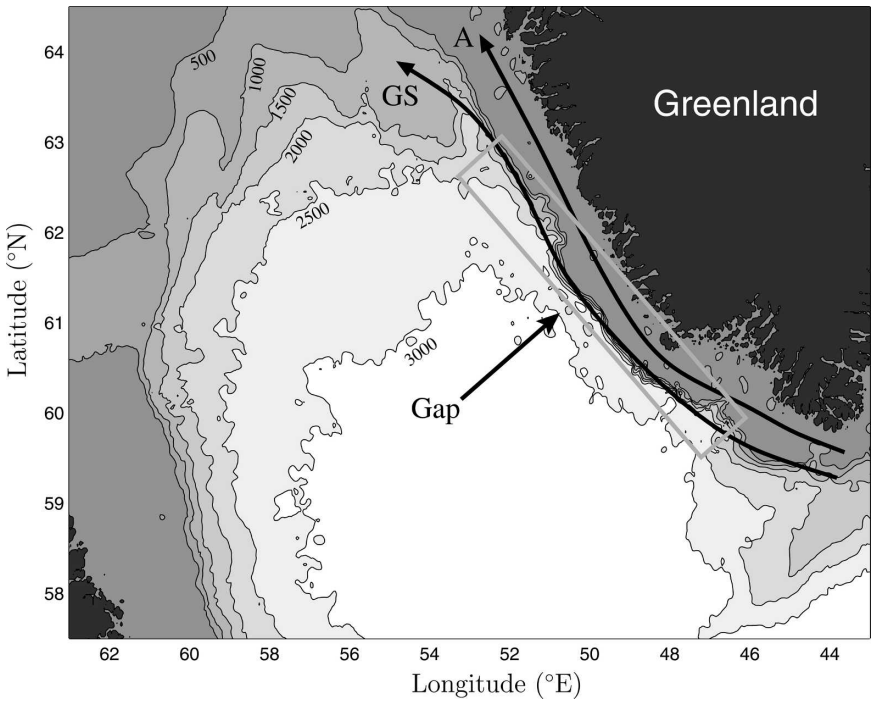

FIG. 1. Bathymetry of the Labrador Sea basin. Depth contours are given at 500-m intervals. The arrows give the paths of two components of the West Greenland Current. The path of the fresh, Arctic-origin shelf water is labeled "A," and the path of the salty, Gulf Stream–origin slope water is labeled "GS."

the gap. The WGC is forced to pass over this change in bathymetric slope, that is, over the gap, as illustrated schematically in Fig. 1.

The WGC is associated with a region of enhanced eddy variability centered at 61°N, 52°W, near where the 3000-m isobath diverges from the coast at the downstream end of the gap. This region of variability is evident in satellite altimetry records (Prater 2002; Lilly et al. 2003), and in the tracks of surface drifters (Cuny et al. 2002) and RAFOS floats (Prater 2002). Eddies present in this region are called "Irminger rings" and are filled at middepth with warm, salty Gulf Stream–origin water; they often contain cold, fresh Arctic-origin water near the surface (Prater 2002; Lilly et al. 2003), as well. Buoyant shelf and slope water is carried into the interior of the Labrador Sea when the eddies detach from the current. This lateral flux of buoyant water is thought to be a mechanism by which the Labrador Sea rapidly restratifies after winters of intense deep convection (Katsman et al. 2004).

The eddy formation rate is apparently not coupled to changes in the local winds (Pickart et al. 2002), and the proximity of the region of high eddy kinetic energy to a major bathymetric feature suggests that the eddies are generated by an internal instability of the WGC triggered by changes in the bathymetry (Eden and Böning 2002; Bracco and Pedlosky 2003; Katsman et al. 2004). Indeed, the eddy kinetic energy maximum is at the downstream end of the 470-km-long bathymetric gap where the continental slope narrows significantly and the value of the slope exceeds 0.15 (as measured from the 500–2500-m isobaths). Upstream and downstream of this gap, the continental slope is wider, with an average slope of about 0.02. Outside of the bathymetric gap, the WGC is stable, and no eddy formation is observed (Prater 2002).

It is possible that the curvature of the bathymetry west of Greenland or the sudden divergence of the 3000-m isobath from the coast around 61°N also affect the stability of the WGC. However, the models of Katsman et al. (2004), which produces Irminger rings without either of these effects, and Eden and Böning (2002), which shows significant eddy formation at the upstream end of the gap, imply that these two factors play—at most—a secondary role in the formation of Irminger rings. Rather, it is clear that changes in the width and steepness of the continental slope are the primary influence on the stability of the WGC.

The effect of sloping topography on a baroclinically unstable, inviscid, quasigeostrophic model has been studied by Blumsack and Gierasch (1972) and Gill et al. (1974). These studies found that a current flowing over

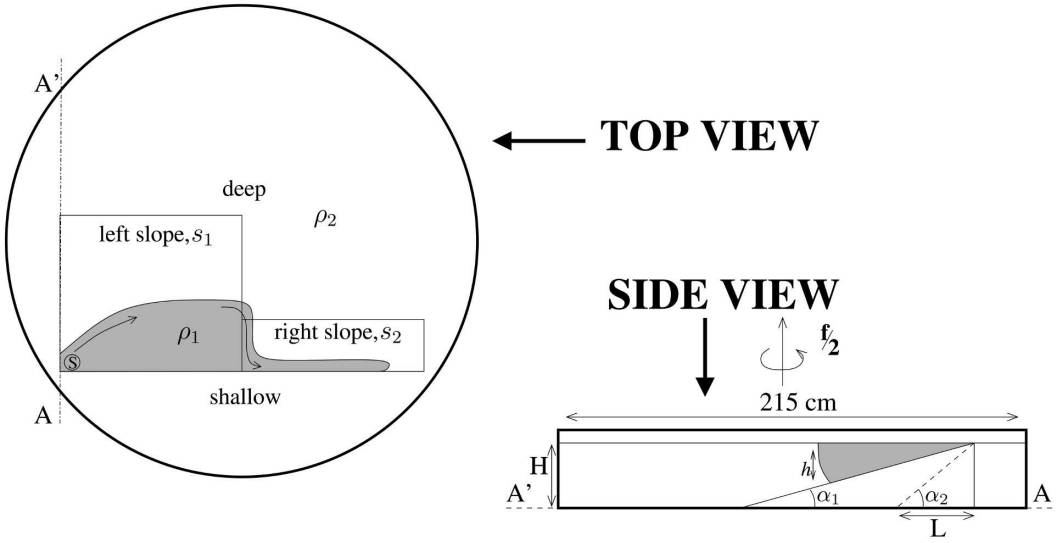

FIG. 2. Experimental apparatus used in the half-gap experiments: (left) top view and (right) side view. The arrows indicate the flow direction.

topography that slopes in the opposite direction as the isopycnals (as is the case with a buoyant coastal current) is always unstable, but that the growth rates of unstable waves are much lower than with a flat-bottom topography. Subsequent studies of oceanic fronts using increasingly more realistic models have confirmed this basic result (Flagg and Beardsley 1978; Gawarkiewicz 1991; Spall 2004). Rotating table experiments by Condie (1993) and Cenedese and Linden (2002) have shown that, in addition to delaying the onset of instabilities, strongly sloping bathymetry can also prevent the instabilities that appear from growing to large amplitudes and forming eddies.

The effect of a bathymetric gap like that found in the path of the WGC on the stability of a buoyant coastal current has been less studied. Bracco and Pedlosky (2003), building on a study by Samelson and Pedlosky (1990), investigated the nonlinear stability of a two-layer, quasigeostrophic channel flow over a stabilizing bottom slope throughout most of the channel that was interrupted by a gap containing a destabilizing slope. They found that coherent vortices were formed in the gap and ejected into the exterior flow; this occurred for all gaps greater than one Rossby radius. The authors suggested that their model could be considered an idealization of the WGC and note the similarity of the coherent vortices formed by their model with the Irminger rings found in the Labrador Sea.

The purpose of this paper is to discuss a series of laboratory experiments designed to further elucidate the conditions under which Irminger rings form by buoyant flow over bathymetry that abruptly narrows and steepens. The geometry of the bathymetry in the experiments is much simpler than in either the Labrador Sea or any of the numerical models aimed at simulating the formation of Irminger rings, and it is hoped that this simplification sheds additional light on the problem. The experiments are divided into two sets. In the first set, the "half gap" experiments, we allow a buoyant current to flow from a gentle slope onto a steep slope, or from a steep slope onto a gentle slope. These experiments, which model the upstream and downstream ends, respectively, of the bathymetric gap over which the WGC flows, seek to address which process is more important in the formation of Irminger Current eddies and how the steepness of the destabilizing slope effects the eddy formation process. The second set of experiments, the "full gap" experiments, investigates whether the length of the bathymetric gap having a steep slope impacts the formation of eddies.

The format of the paper is as follows: in section 2, we will describe the experimental methods. Section 3 will introduce some scales relevant to buoyant coastal currents. Sections 4 and 5 focus on the half-gap and full-gap experiments, respectively. We will compare the results of these experiments with existing theoretical results in section 6 and with observations of Irminger rings in section 7. In section 8, we will summarize our findings.

2. Experimental methods

The half-gap experiments (shown in Fig. 2) were performed in a 215-cm-diameter, 45-cm-deep opaque plas-

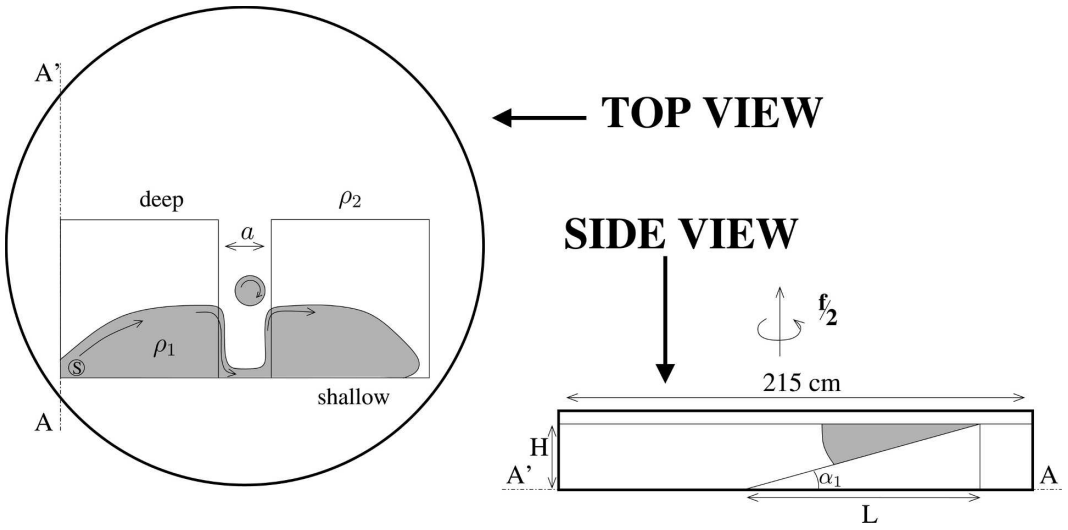

FIG. 3. Experimental apparatus used in the full-gap experiments: (left) top view and (right) side view. The arrows indicate the flow direction. The isolated circle of buoyant fluid represents an eddy that often formed in the gap.

tic tank mounted on a 2-m-diameter direct-drive rotating table with a vertical axis of rotation. The table rotates anticlockwise unless otherwise noted. The tank was filled to a depth of either $H = 15$ cm or $H = 22.5$ cm with a saltwater of density ρ_2. The two slopes were mounted in the tank away from the sidewalls. The lengths of the left-hand (s_1) and right-hand (s_2) slopes (looking downstream) were 72 and 82 cm, respectively, and both slopes were painted with a 10 cm $\times$ 10 cm grid. The left-hand slope was fixed at $s_1 = 0.29$, while the right-hand slope was adjustable from $s_2 = 1.0$ to $s_2 = \infty$. The slope s_i is defined by $s_i \equiv \tan\alpha_i$, where α_i is the angle the ith slope makes with the horizontal. Dyed buoyant water of density $\rho_1 < \rho_2$ flowed from a 1.1-cm-diameter nozzle (marked "S" in the figure) placed about 0.5 cm below the free surface and about 5 cm from the outcrop of the slope (i.e., the "coast"). The nozzle was covered with a piece of sponge to reduce mixing between the buoyant and ambient fluids. The buoyant water flowed onto the left-hand slope where it developed into a buoyancy-forced boundary current that flowed with the coast on its right (looking downstream). In this configuration, the current originates on the gentle slope and flows onto the steep slope, simulating the upstream end of the gap. For the experiments modeling the downstream end of the gap, the current should flow from the steep slope onto the gentle slope. Rather than physically reverse the slopes, the source was simply moved to the far end of the right-hand slope and table was rotated clockwise. The current then flowed from right to left, with the coast on the left (looking downstream).

The buoyancy force on the current is proportional to the reduced gravity $g' = g(\rho_2 - \rho_1)/\bar{\rho}$, where g is the gravitational acceleration and $\bar{\rho} = (\rho_2 + \rho_1)/2$. The reduced gravity was calculated using the densities of the fluids before the beginning of the experiment. The actual value of the reduced gravity was reduced somewhat by mixing. Sampling of buoyant water from the developed current revealed that g' was reduced in the experiments by between 20% and 50%. In these experiments, the input reduced gravity was kept fixed at $g' \approx 1$ cm s^{-2}. The magnitude of the Coriolis parameter $|f|$ varied from 0.5 to 2.0 s^{-1}, but was usually fixed at $|f| = 2.0$ s^{-1}. The flow rate was fixed at $Q = 12$ cm^3 s^{-1}, except for one experiment in which $Q = 6.0$ cm^3 s^{-1}.

The full-gap experiments (shown in Fig. 3) were performed in the same tank as the half-gap experiments, using two identical slopes with $s = 0.29$ separated by a gap of variable length a. The shoreward side of the gap was a vertical wall. In all other respects, these experiments were identical to the half-gap experiments. The gap length a took on values of 1, 5, 10, 20, and 40 cm. All other parameters were kept fixed with $g' = 1$ cm s^{-2}, $f = 2.0$ s^{-1}, and $Q = 12$ cm^3 s^{-1}.

For all of the above experiments, a top view of the flow was recorded using a video camera that was corotating with the table. The current was made visible by the addition of food coloring and, in several experiments, surface velocities were obtained by floating paper pellets on the surface. The width of the current (i.e., the distance from the coast to the surface outcrop of the buoyant current) was measured by eye by looking at the dye concentration. The 10 cm $\times$ 10 cm grid painted on the slopes allowed the width of the current to be determined to an accuracy of about 1 cm. Width mea-

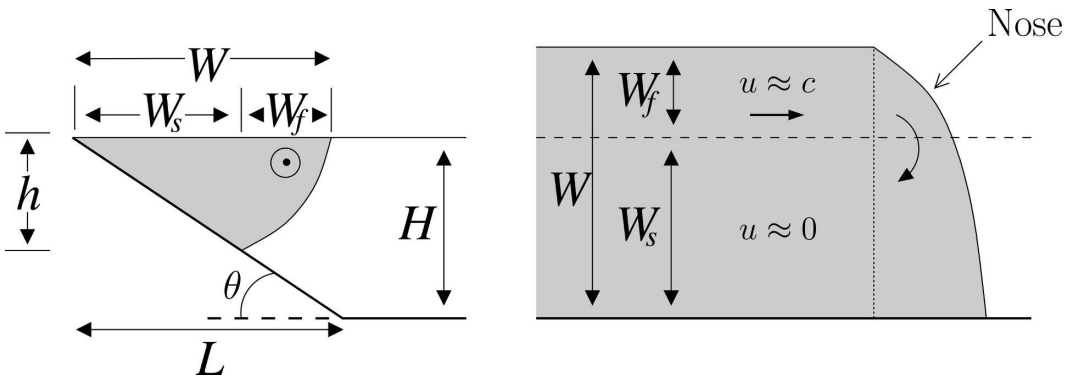

FIG. 4. Schematic (left) cross section and (right) top view of a buoyant coastal current flowing along sloping bathymetry with slope $s = \tan\theta = H/L$, after Lentz and Helfrich (2002), their Fig. 3.

surements were obtained at three locations separated by 20 cm on each slope, starting at 20 cm downstream from the source on the left-hand slope or 20 cm downstream from the point where left- and right-hand slopes meet. The reported widths are the average of these three measurements.

3. Review of relevant dynamical scales

Before describing the experiments in detail, it is useful to examine some relevant scales and balances for the buoyant currents considered here. As with many coastal flows, this problem is asymmetric, requiring two separate Rossby numbers, Ro_x and Ro_y, to describe the alongshore and cross-shore momentum balances, respectively. The two Rossby numbers differ by the square of the horizontal aspect number and have the values

$$\mathrm{Ro}_x \sim 0.1\text{–}1 \quad \text{and} \quad \mathrm{Ro}_y \sim 0.001\text{–}0.01. \tag{1}$$

Given the smallness of the cross-shore Rossby number, the cross-shore momentum equation is an approximate balance between the Coriolis force and the pressure gradient force (and possibly viscosity, discussed later). This balance will break down near the point where the two slopes meet and inside the "gap," but it is expected that the current will reacquire geostrophic balance within a few Rossby radii of where the two slopes meet.

Several authors have proposed scale variables that can be used to classify buoyant coastal currents using parameters that can be controlled or measured at the source. The most convenient for the purposes of this study are those derived and tested in a series of laboratory experiments by Lentz and Helfrich (2002). An idealized representation of the flow studied by these authors is shown in Fig. 4. The current is assumed to behave like a two-layer Margules front with all of the transport Q confined to a region of width W_f between where the front intersects the bottom (the foot) and the surface (the outcrop). The fluid in contact with the bathymetry has width W_s and is assumed to be quiescent after the passage of the nose of the current. The primary measured quantity in the present experiments is the total width of the current $W = W_s + W_f$.

The scales for the depth of the foot, the width of the quiescent region, the width of the front, the current speed seaward of the foot, and the speed of the nose of the current are

$$h \sim \sqrt{\frac{2Qf}{g'}}, \tag{2}$$

$$W_s \sim h/s, \tag{3}$$

$$W_f \sim R_D = \frac{\sqrt{g'h}}{f}, \tag{4}$$

$$u \sim c = \sqrt{g'h}, \quad \text{and} \tag{5}$$

$$c_n \sim c\left(1 + \frac{h}{sR_D}\right)^{-1}, \tag{6}$$

respectively. The first of these scales is the trapping depth for a coastal density front introduced by Chapman and Lentz (1994), while the second follows from the geometry of the wedge of current shoreward of the foot. The third and fourth scales are simply the Rossby radius R_D and internal gravity wave speed c based on the depth of the foot of the front h, respectively. The final scale, the nose speed c_n, was proposed by Lentz and Helfrich (2002) based on considerations of volume conservation in the nose of the current. Note that while the fluid velocity seaward of the front scales with c, the nose speed c_n is much smaller because moving fluid must turn once it reaches the nose to fill the wedge of quiescent fluid shoreward of the foot. Values of these

scales for typical values of the input parameters are given in Table 1.

The quantity $s' = h/R_D$ is an estimate of the isopycnal slope of the front, and its ratio with the topographic slope s defines an inverse slope Burger number, which is an important parameter for predicting the behavior of the current over sloping bathymetry (Yankovsky and Chapman 1997). With the definition of s', the current nose speed can be written $c_n = c(1 + s'/s)^{-1}$, which makes it clear that if $s'/s \gg 1$ ($s'/s \ll 1$) then $c_n \ll c$ ($c_n \approx c$).

The impact of viscous effects on the buoyant current can be quantified by the Ekman number Ek. As with the Rossby number, the asymmetry in the horizontal length scales requires two Ekman numbers, differing by the square of the aspect ratio. The alongshore and cross-shore Ekman numbers are

$$\mathrm{Ek}_x \sim 0.1 \quad \text{and} \quad \mathrm{Ek}_y \sim 10^{-3}-10^{-2}, \tag{7}$$

respectively. Both Ekman numbers are small, so viscosity is not expected to enter the momentum balance at first order, justifying the assumption that the front is geostrophically balanced. The effects of viscosity manifest themselves in a slow offshore movement of the surface outcrop over the course of many rotation periods. The foot remains fixed as the current widens, so the velocity of the current must decrease to conserve the total flux of buoyant fluid. The spreading mechanism has not been definitively explained, but Lentz and Helfrich (2002) suggest that it may result from an offshore flux of water in an interfacial Ekman layer between the buoyant and ambient waters.

4. Half-gap experiments

a. Results

1) Gentle to steep slope

Seventeen experiments were performed in which the buoyant current was allowed to equilibrate on a gentle slope then flow onto a steep slope, thus modeling the upstream end of the bathymetric "gap" west of Greenland. The total width of the current was much larger on the gentle slope than on the steep slope (because of the larger value of W_s). The passage of the nose often trapped some dense ambient fluid between the current and the coast and the resulting density contrast drove a weak flow along the shoreward edge of the current toward the source. This shoreward front was extremely susceptible to instabilities that smoothed out the shoreward edge of the front, but they did not appear to effect the large-scale evolution of the current. These instabilities are visible in Figs. 5a and 5b and disappeared as the current filled the space between the foot and the shore (Figs. 5c and 5d). No eddies were observed to form on the gentle slope.

When the nose of the current passed from the gentle slope to the vertical wall, it shed a small wisp of fluid (marked by the white arrow in Fig. 5a) extending into the ambient fluid. This initial perturbation propagated more slowly than the nose of the current and grew rapidly into a large anticyclonic eddy about 20 Rossby radii (25 cm) downstream of the beginning of the vertical wall. This eddy consumed much of the flux along the vertical wall and delayed the formation of further instabilities downstream of the eddy. Other instabilities eventually grew and formed eddies, the beginnings of which are seen in Figs. 5c and 5d. Formation of a large eddy immediately downstream of the gentle slope was a particular feature of buoyant intrusion onto the vertical wall and was not observed for large but finite slopes.

When the nose of the current flowed from a gentle slope to a steep but not vertical slope the flow was initially steady and laminar. As the experiment progressed the surface outcrop of the current moved slowly offshore because of the frictional effects discussed in section 3 and the current developed occasional meanders, but the growth to large amplitude and the development of eddies was delayed until the current was wider than the slope and the surface outcrop of the current lay over the flat bottom of the tank. When instabilities did occur, they appeared along the entire length of the right-hand slope simultaneously (Figs. 6c and 6d). This behavior was observed on all slopes with $1 < s_i < \infty$ (if $s_i \leq 1$ the current never widened sufficiently during the course of the experiment to be wider than the slope). The wavelength of the initial disturbances was about 6–8 Rossby radii, which, if conditions were favorable, would grow into a pair of eddies with a diameter of 3–4 Rossby radii each.

To isolate the effect of the slope width, a series of experiments were performed wherein the depth H of the ambient fluid was increased to 22.5 from 15.0 cm, but the slopes were unchanged. This increased the width of the sloping bathymetry without changing its

TABLE 1. Values of the scale variables h, R_D, and c given by representative values of the input variables Q, g', and $|f|$.

Q	12.0 cm^3 s^{-1}
g'	1.0 cm s^{-2}
$\|f\|$	2.0 s^{-1}
h	6.9 cm
R_d	1.3 cm
c	2.6 cm s^{-1}
s'	5.3

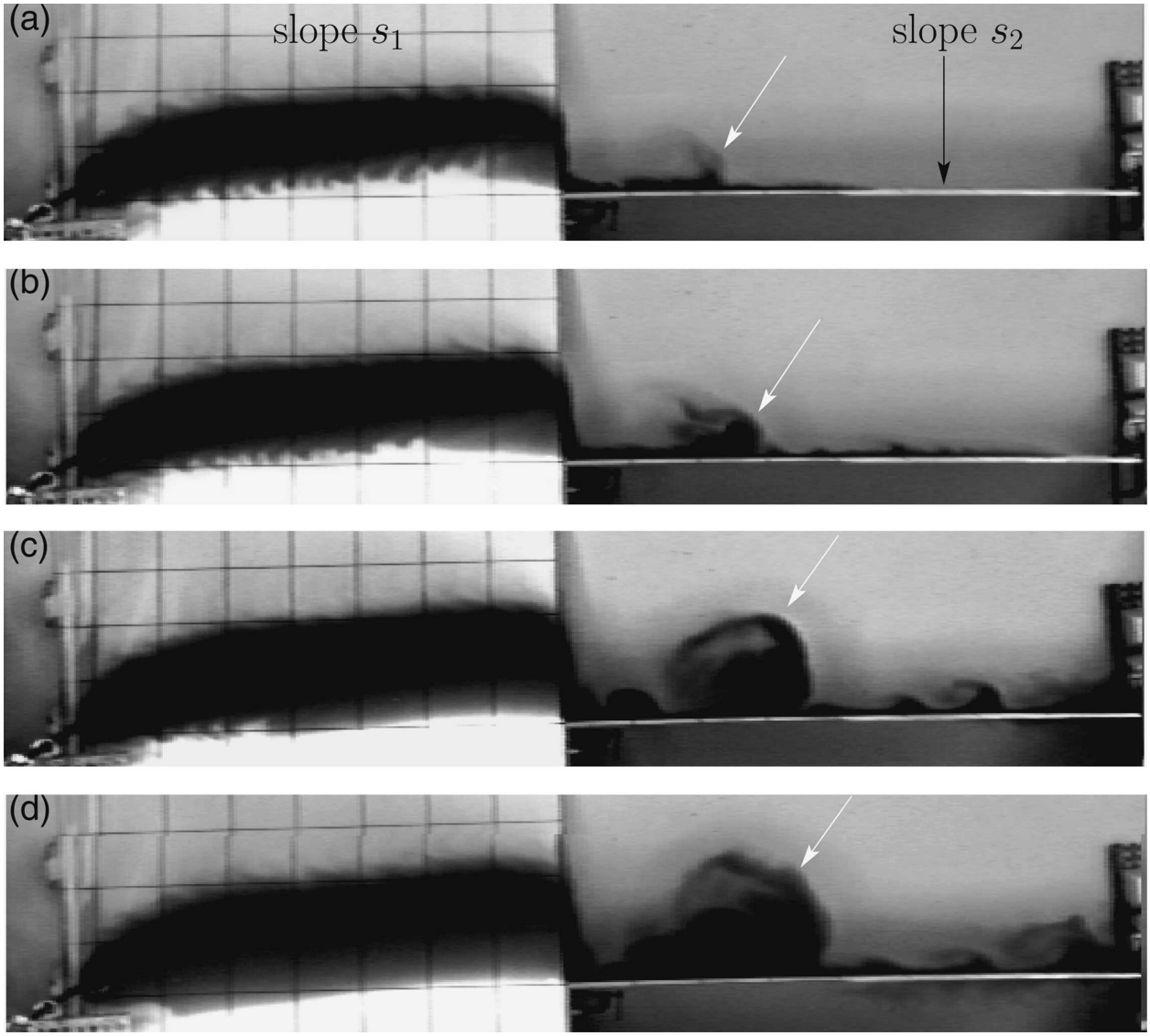

FIG. 5. Top view of a buoyant current ($Q = 12.0\ \text{cm}^3\ \text{s}^{-1}$, $f = 2.0\ \text{s}^{-1}$, $g' = 0.78\ \text{cm}\ \text{s}^{-2}$, $s_1 = 0.29$, $s_2 = \infty$, $s' = 6.1$) flowing from (left) a gentle slope to (right) a vertical wall after (a) 240, (b) 288, (c) 408, and (d) 504 s. See Fig. 2, left panel, for orientation. Note the formation of a large eddy, denoted by a white arrow, on the vertical wall.

slope. In these experiments, the formation of eddies was again delayed until the surface outcrop of the current extended beyond the slope, implying that the relative width of the bathymetry to the current was more important in determining stability that the value of the slope itself.

The evolution of all currents that formed eddies over steep bathymetry is summarized in Fig. 7, showing that eddies only formed once the current was wider than the sloping bathymetry. In Fig. 8, we plot the width of the current just before eddies begin to form, as well as the width of the current at the end of the experiment if it remained stable, versus the width of the slope. Again, all of the eddying currents fall above the line $W = L$. The width of the currents just before eddy formation is well fit by the line $W = L + (1.6 \pm 0.6)R_D$, shown as a dashed line in Fig. 8, implying that the currents tended to form eddies when the width of the current exceeded that of the slope by 1.6 ± 0.6 Rossby radii.

2) STEEP TO GENTLE SLOPE

In the second set of experiments, a buoyant current flowed from a steep slope onto a gentle slope. Again, the current was narrower on the steep slope than on the gentle slope. The current was initially stable on the steeper slope and remained stable as it flowed onto the

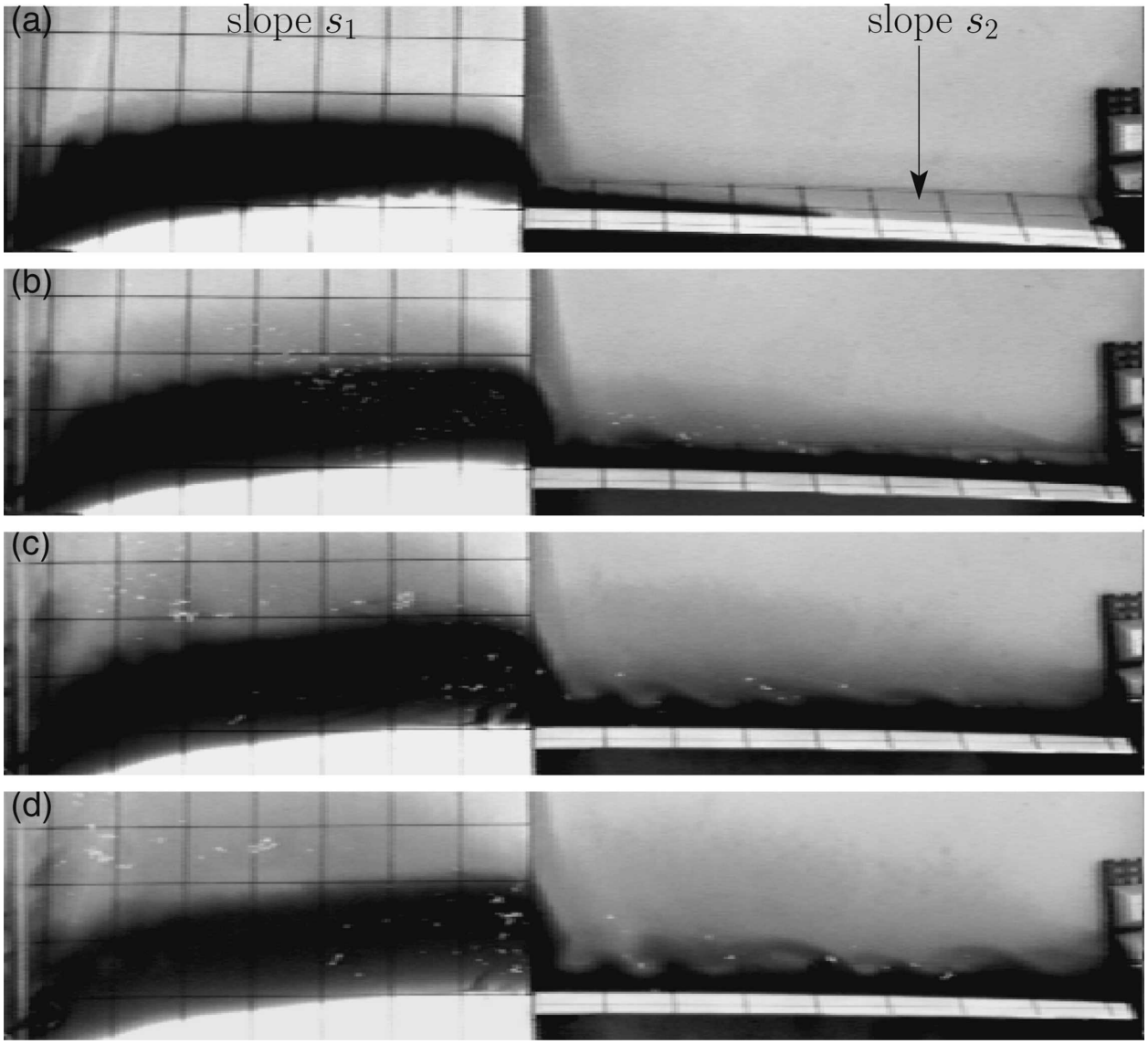

FIG. 6. Top view of a buoyant current ($Q = 12.0$ cm^3 s^{-1}, $f = 2.0$ s^{-1}, $g' = 1.0$ cm s^{-2}, $s_1 = 0.29$, $s_2 = 3.7$, $s' = 5.3$) flowing from (left) a gentle slope to (right) a steep slope after (a) 124, (b) 279, (c) 465, and (d) 589 s. See Fig. 2, left panel, for orientation.

gentle slope (Figs. 9a and 9b). Once the current widened sufficiently that its surface outcrop lay beyond the sloping bathymetry of the steep slope, it became unstable and began to form eddies. However, even if the current was initially meandering or forming eddies, it was immediately stabilized on the gentle slope. Eddies that formed on the steep slope did not propagate onto the gentle slope, and accumulated at the downstream end of the steep slope as (Figs. 9c and 9d). The flux of buoyant fluid onto the gentle slope was reduced by the shedding of eddies along the steep slope, resulting in a current that was narrower and slower on the gentle slope than those seen in the "gentle to steep slope" experiments. Aside from this minor difference, the current on the gentle slope in these experiments was nearly identical to that observed in the previous experiments.

b. Discussion

The current did not become unstable on the steep slope until it had widened beyond the slope width. Once this had happened, instabilities appeared along the entire length of the slope almost simultaneously, implying that the instability on the steep slope was purely local phenomenon: the current became unstable if local conditions were favorable for instability regardless of the upstream conditions. The abrupt change in bathymetry required a rapid, ageostrophic adjustment of the current, but the adjustment was accomplished

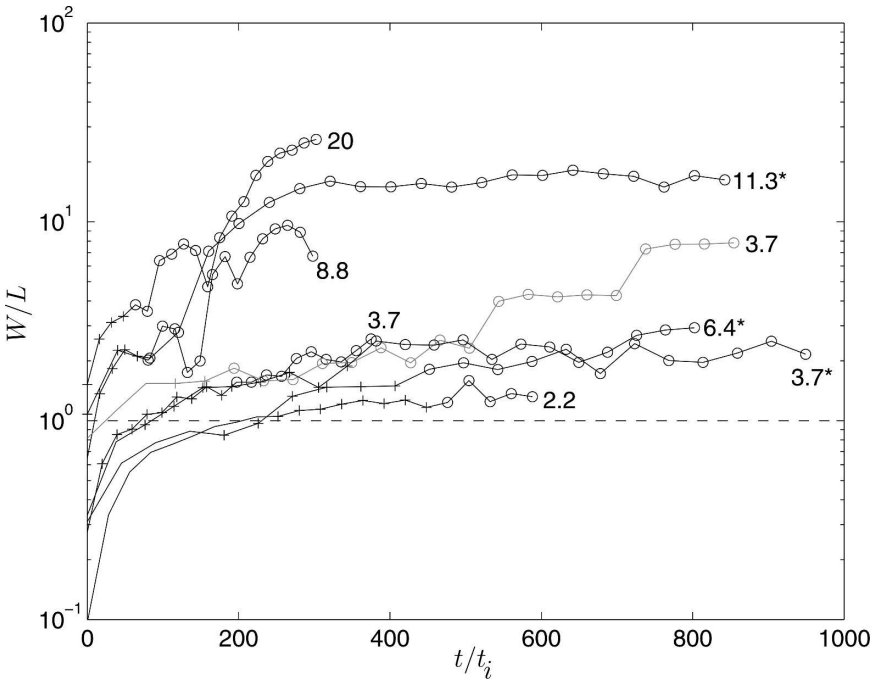

FIG. 7. The total width W normalized by slope width L vs time for currents on a slope that eventually formed eddies (see Fig. 4 for the definition of W and H); $t_i = f/\pi$ is the inertial period, and pluses and open circles indicate whether the current is meandering or forming eddies, respectively. Numbers at the end of each curve give the slope over which each current formed. Those with asterisks have total depth $H = 22.5$ cm; those without have $H = 15.0$ cm. Note: this figure also contains data (shown in gray) from the steep to gentle slope experiments [section 4a(2)].

without introducing instabilities into the current. This was not true in the exceptional case of the vertical wall, which had a singular limit of a steep slope. Here the behavior is qualitatively different, because the initial adjustment of the nose of the current introduced a perturbation that grew to large amplitude and dominated the subsequent evolution of the current. It is not clear how this eddy formation mechanism is relevant to the WGC, because this current does not take the form of an intrusion with a well-defined nose.

When the current flowed from the steep to the gentle slope, the abrupt widening of the isobaths neither introduced instabilities onto the gentle slope nor influenced the evolution of the current upstream of the change in bathymetry, except to serve as an accumulation point for eddies generated on the steep slope. The instability over the steep slope was again a purely local phenomenon and was not influenced by the abruptness of the change in bathymetry.

As was pointed out by a reviewer, the abrupt transition between the two slopes may have launched inertial waves because the alongshore Rossby number was not small. These waves would have a wavelength $U/f \sim 1$ cm and would propagate a horizontal distance approximately equal to the depth of the fluid (e.g., Hide et al. 1968). Because the fluid depth at the slope transition ranged from 0–15 cm, it is unlikely that these waves had a strong influence on the eddies formed far downstream of the slope transition. The one case where inertial waves may have played a crucial role in the formation of eddies was in flow from the gentle slope to the vertical wall. In that case, the large eddy that formed immediately downstream of the slope transition may have been triggered by inertial waves, or some other local, ageostrophic phenomenon. However, a detailed consideration of the ageostrophic effects occurring in the transition region is beyond the scope of this study.

The sloping bathymetry always had a stabilizing influence, with the current always locally more stable on a slope than on a vertical wall. Additionally, the sloping bathymetry used in the experiments prevented the formation of eddies until the current was wider than the bathymetry and the surface outcrop (the part of the current most active in the instability) was over the flat bottom of the tank. The current can then be thought of as a narrower current of effective width W^* flowing along a vertical wall. The relationship of W^* to the measured width W can be determined by attempting to

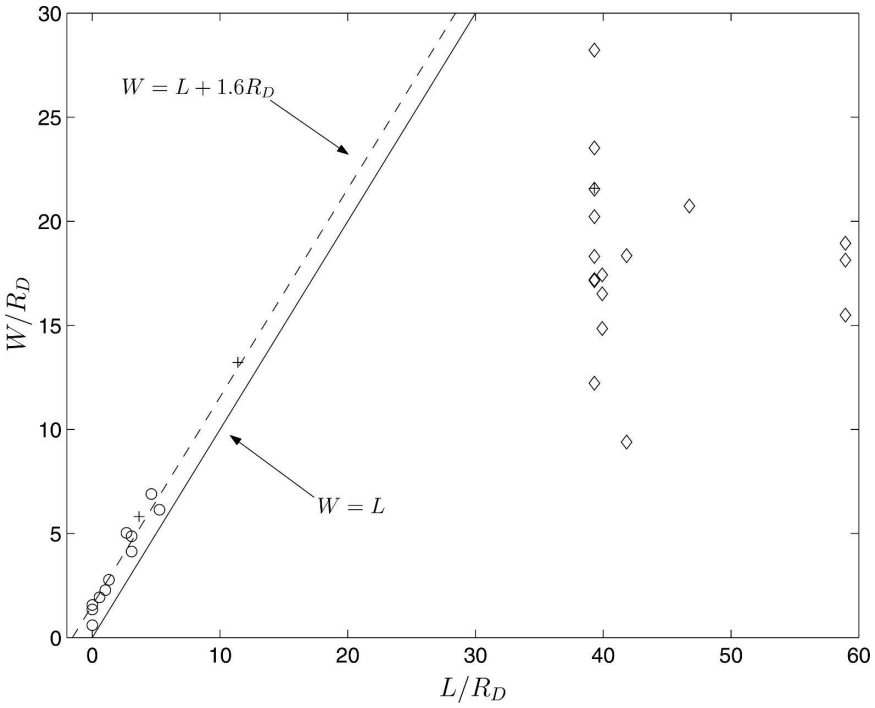

FIG. 8. Final width of current vs shelf width $L = H/s$, both normalized by the Rossby radius, for all half-gap experiments; diamonds, pluses, and circles indicate that the current was steady, meandering, or forming eddies, respectively. For currents that formed eddies, the final width was measured just before eddies began to form.

reconcile the results of the current experiments with those of Cenedese and Linden (2002), which used a flat continental shelf separated from a flat-bottomed "abyss" by a vertical wall. They found that the current became unstable when it exceeded the width of the shelf by 2–6 Rossby radii, while the currents in the present experiments became unstable when they exceeded the slope width by 1.6 Rossby radii. If we assume effective width can be written $W^* \approx W - L + \alpha R_D$, where L is the width of the sloping bathymetry, we may choose the empirical parameter to reconcile the present results with those of Cenedese and Linden (2002). The value of α must be between 0.4 and 4.4 to have $W^* = 2$–$6R_D$, but, at present, we do not have any theoretical or observational evidence that would allow us to further refine this value.

Consideration the potential vorticity dynamics of the ambient fluid provides a straightforward explanation for the stabilization of currents by a bottom slope. The formation of eddies distorts the outcrop of the front and requires cross-shore displacement of ambient fluid columns. If the outcrop lies over a flat bottom this motion can be accomplished without change in the relative vorticity of the fluid columns. When the outcrop lies over a sloping bottom, however, the displacement forces the fluid columns across isobaths, which is suppressed in near-geostrophic motion and requires that the fluid columns develop relative vorticity at an energy cost to the growing eddies; the steeper the slope, the greater the relative vorticity developed by the ambient fluid and the greater energy cost to sustain those motions. Thus, strongly sloping topography can be expected to sharply reduce the growth rate of growing disturbances to the buoyant current and lead to current stabilization.

In summary, the narrowing of the bathymetry in the gentle to steep slope experiments created conditions favorable for eddy formation by reducing the offshore distance the surface outcrop had to move before it lay over the flat bottom of the tank. The abruptness of the transition was important only in case of flow onto a vertical wall. The sudden widening of the slope in the steep to gentle slope experiments merely served as an accumulation point for the eddies formed upstream. The current downstream of this point was always stable, regardless of its conditions upstream.

5. Full-gap experiments

a. Results

This set of experiments was designed to determine if the length of the bathymetric gap affected the eddy

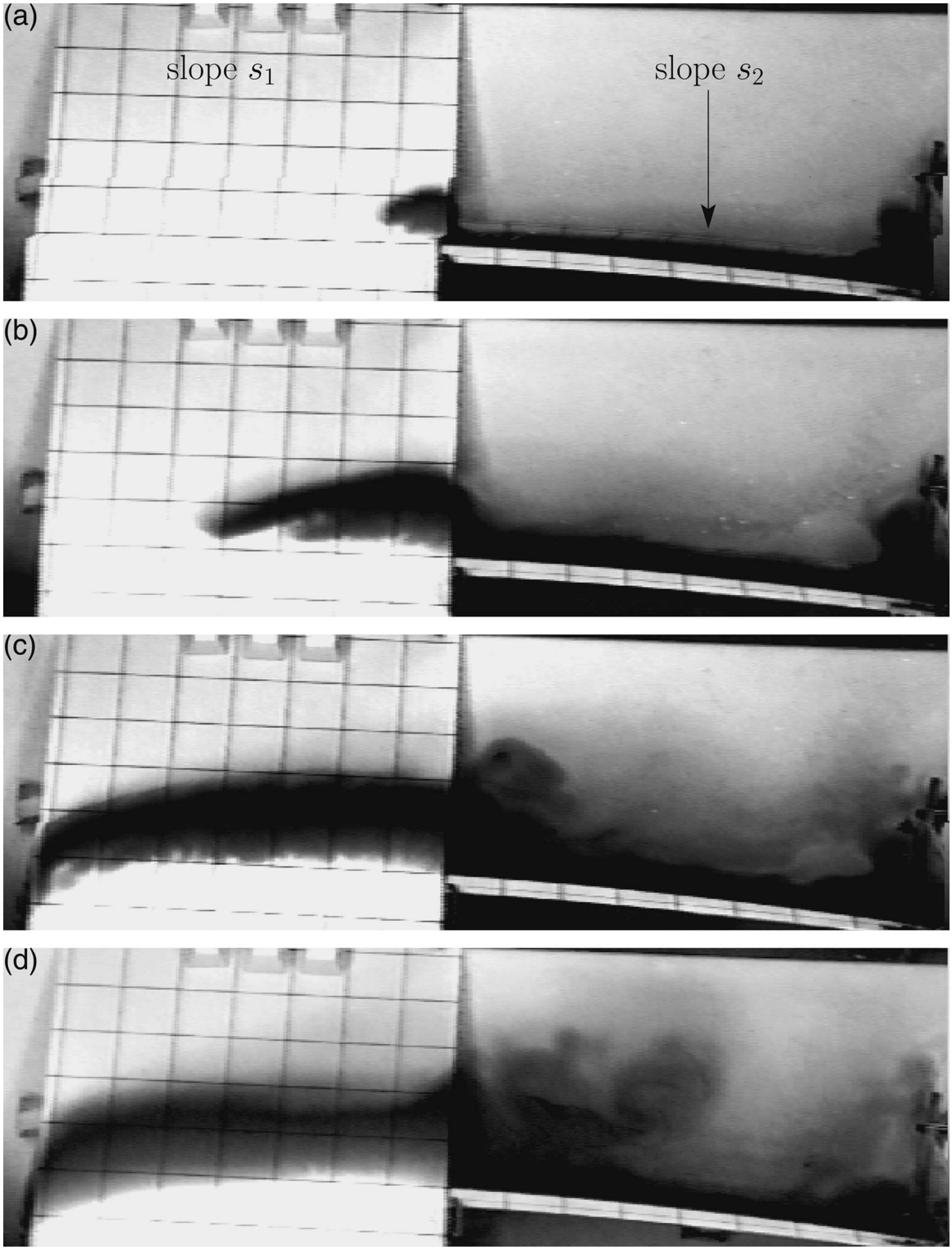

FIG. 9. Top view of a buoyant current ($Q = 12.0\ \text{cm}^3\,\text{s}^{-1}$, $f = -2.0\ \text{s}^{-1}$, $g' = 1.0\ \text{cm}\,\text{s}^{-2}$, $s_1 = 0.29$, $s_2 = 3.7$, $s' = 5.3$) flowing from (right) a steep slope to (left) a gentle slope after (a) 122, (b) 305, (c) 607, and (d) 1037 s. See Fig. 2, left panel, for orientation. Note that the current flows from right to left because $f < 0$.

formation rate. The experiments were performed with gap sizes ranging from $a = 1$ cm to $a = 40$ cm (see Fig. 3), corresponding to $a = 0.8R_D$ to $a = 32R_D$, where R_D is the Rossby radius of deformation given by Eq. (4). As described in section 2, the gap had a vertical wall on the shoreward side, while upstream and downstream of the gap the current flowed over a gentle slope. For experiments with $a \leq 4R_D$, the flow within the gap exhibited small perturbations that decayed downstream of the gap over the gentle slope, but no eddy formation was observed. Once the gap size was increased to $a = 8R_D$, eddies began to form in the gap. Two stationary coherent eddies formed in the gap when $a = 8R_D$: a cyclonic eddy of ambient fluid near the wall and an anticyclonic eddy of buoyant fluid seaward of the first eddy. When the gap was increased to $a = 16R_D$ three eddies formed, with a cyclonic–anticyclonic pair occupying the same positions as before and an additional cyclonic eddy seaward of the anticyclonic eddy. The eddy pair was stationary throughout the experiment, while the third cyclonic eddy migrated back and forth across the gap, sometimes closer to the upstream end of the gap, at other times closer to the downstream end of the gap. The experiment with the largest gap ($a = 32R_D$, shown in Fig. 10) developed a random field of cyclonic and anticyclonic eddies where the number of eddies increased as the experiment proceeded. By the end of the experiment, at least seven individual eddies had formed.

In none of the full-gap experiments were eddies that formed in the gap able to propagate onto the gentle slopes, either upstream or downstream of the gap. Eddies advected downstream in the gap accumulated at the downstream end of the gap rather than propagating onto the slope. In the experiment with the largest gap, the eddies that accumulated at the downstream end of the gap were gradually forced offshore by the continual formation of new eddies near the coast (Fig. 10).

b. Discussion

The length of the gap had a profound influence on the number of eddies formed and on their formation rate. The gap had to exceed a critical length $a_c > 4R_D$ before eddies would form at all. Even then, the eddy field saturated to only a few eddies unless the gap was longer than a second critical length $a_c' > 16R_D$. Recall that, in the half-gap experiments, the wavelength of the initial disturbances was observed to be $6–8R_D$. Thus, eddies were unable to form in the gap until its length exceeded the wavelength of the initial growing disturbances. For $a_c < a \leq a_c'$ individual eddies occupied a large fraction of the space inside the gap and were able to simultaneously interact with both sides of the gap, the boundary current encircling the gap, and each other. This interaction was sufficiently strong to trap the eddies at a fixed location and to stabilize the boundary current against further eddy formation. Once the gap length exceeded approximately two wavelengths (or four eddy diameters), the eddies were no longer trapped and could move away from the boundary current, allowing new eddies to form.

6. Comparison with previous theory and experiments

The effect of sloping bathymetry on the stability of a front is a classic problem with a long history. A fundamental stability criterion was derived by Pedlosky (1964): a necessary condition for a geostrophic front to become unstable is that the gradient of the potential vorticity charges sign across the front. This condition is always satisfied by a surface to bottom front like those considered here and, indeed, such a front is always unstable over a flat bottom (Orlanski 1968). The presence of bathymetry that slopes in the opposite direction as the front increases the potential vorticity gradient contrast across the front and one is naïvely lead to expect that this situation should be more unstable than that of a front over a flat bottom. However, the instability condition is *necessary*, not *sufficient*, and thus cannot be used to predict instability, much less assess relative stability. This can only be determined by a direct calculation or experiment using the geometry of interest.

As discussed in the introduction, a long series of increasingly realistic theoretical studies (Blumsack and Gierasch 1972; Gill et al. 1974; Flagg and Beardsley 1978; Gawarkiewicz 1991) have concluded that the presence of sloping bathymetry has a strong stabilizing influence on the front, relative to a flat bottom, and this stabilization became stronger as the slope increased. This effect has also been observed in the continuously stratified, eddy-resolving, primitive equation numerical model used by Spall (2004). Thus, the fact that the sloping bathymetry had a stabilizing influence in the current experiments was anticipated by numerous theoretical and numerical models.

Several laboratory experiments have also addressed the stability of a buoyant current over sloping bathymetry. Cenedese and Linden (2002) performed a series of ring-source experiments with a flat, axisymmetric continental shelf joined to a continental slope with a fixed slope of 0.5. The parameter range considered was very similar to that used in the present experiments. They found that the sloping bathymetry prevented wavelike disturbances on the seaward edge of the front from growing to large amplitudes. Instead, they would eventually decay and the current would regain axisymmetry.

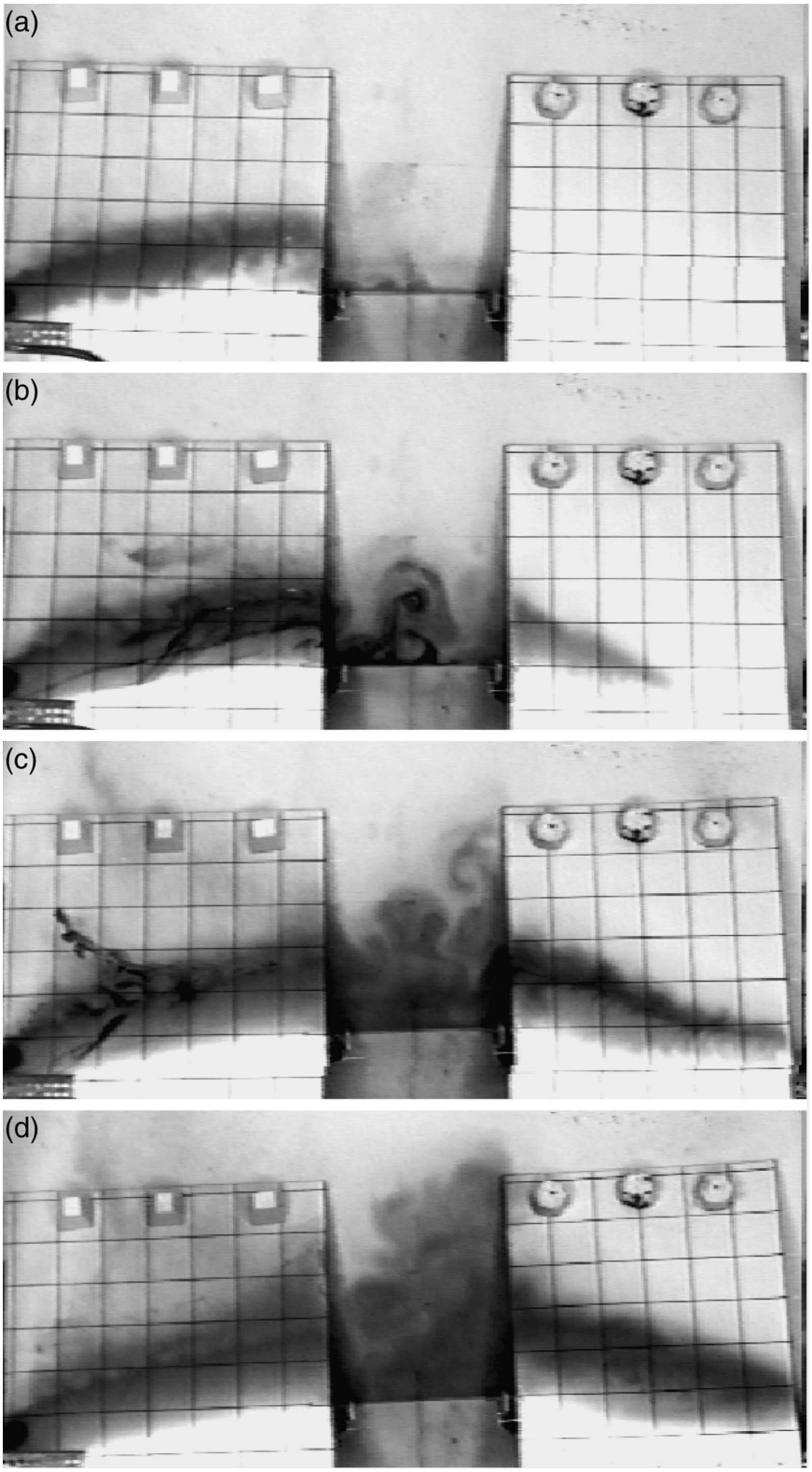

FIG. 10. Top view of a full-gap experiment, with the current ($Q = 12.0$ cm^3 s^{-1}, $f = 2.0$ s^{-1}, $g' = 1.0$ cm s^{-2}, $s = 0.29$, $s' = 5.3$, $a = 40$ cm) flowing from left to right across a gap after (a) 372, (b) 837, (c) 1302, and (d) 1767 s. Darker dye was occasionally injected to help to visualize the flow field. See Fig. 3, left panel, for orientation. Note that the eddies pile up at the downstream edge of the gap. The pyramidal and circular objects on the seaward edges of the slopes are lead weights.

The profound stabilizing influence of sloping topography was also noted by Condie (1993), who used bathymetry with a quadratic profile, but with parameters that were otherwise similar to those in the present experiments. Laboratory experiments require a very different set of assumptions and approximations than theoretical or numerical models, so the fact that sloping bathymetry is observed to have a stabilizing influence in all three types of models demonstrates that this result is remarkably robust.

The stability of flow over a bathymetric gap similar to the full-gap experiments has been studied by Samelson and Pedlosky (1990) and Bracco and Pedlosky (2003). Their studies use a two-layer, quasigeostrophic zonal channel model with a uniform background flow in the upper layer. The channel had a stabilizing bottom slope throughout most of the channel, except for a small along-channel interval where the slope was reduced to zero. The instability mechanism was constrained to be baroclinic by the configuration of their models. Samelson and Pedlosky's (1990) study was restricted to flows with no meridional variation and thus to linear dynamics, whereas Bracco and Pedlosky's (2003) study made no such restriction and allowed nonlinear dynamics. Both studies conclude that the instability is purely local and is not influenced by the stability of the flow outside of the region of instability or the abruptness of the transition. The nonlinear theory predicts a transition in the qualitative form of the instability as the gap size is increased. For gap lengths on the order of R_D [the smallest gap considered in Bracco and Pedlosky (2003)], the gap launched Rossby waves that propagated downstream and decayed outside of the unstable interval. When the gap length was increased to $4R_D$, and above, the instability took the form of coherent vortices that could escape the gap and propagate for large distances downstream. These studies are not directly analogous to the present laboratory experiments because the assumption of quasigeostrophy precludes many ageostrophic processes that, in a less constrained model, may be triggered by the sharp bathymetric features. However, for the reasons discussed in section 4b, we do not believe that the abruptness of the bathymetry used in the present experiments had a large impact on the results, except for the singular case of a vertical wall.

The present experiments also find the instability to be a purely local phenomenon that was not influenced by the stability of the flow outside of the region of instability or the abruptness of the transition. However, no eddies were observed to form until the gap length was increased to $8R_D$ and the eddies were never able to propagate onto the stabilizing slopes. These experiments lacked the uniform background flow of the theoretical models and the gentle slopes used were still much steeper than those allowed by quasigeostrophic theory. In addition, Bracco and Pedlosky's (2003) bathymetry sloped in the same direction as the isopycnals, in contrast with the present experiments. These differences could explain the disagreement, and it would be interesting to repeat the experiments of Bracco and Pedlosky (2003) using a configuration that would allow a more direct comparison with the current experiments.

7. Comparison with oceanic observations

The topographic and isopycnic slopes used in the present experiments are quite large by oceanic standards and it is necessary to develop a set of scaling variables for the slopes and lengths to facilitate comparison with observations.

We concentrate first on the slope. As mentioned previously, the ratio of the isopycnal slope to the bathymetric slope s'/s is the principle parameter controlling the strength of the interaction between the current and the bathymetry (Yankovsky and Chapman 1997; Lentz and Helfrich 2002). This parameter is large (small) when the bathymetric slope is gentle (steep) relative to the slope of the isopycnals. Comparison of the laboratory slopes s with the west Greenland continental slope can be made using this ratio.

The isopycnal slope associated with the WGC, estimated from the spring hydrographic data given in Pickart et al. (2002), is $s'_{\mathrm{OC}} \approx 3 \times 10^{-2}$–$5 \times 10^{-2}$. Typical values for the slope parameter for the laboratory and the WGC are summarized in Table 2 for the case of the current flowing over the gentle or the steep portions of the slope. The small value of the slope parameter over the steep slope indicate that the bathymetric slope is much steeper than the isopycnal slope in both the laboratory and the WGC. In fact, the west Greenland continental slope was best modeled by the steepest slopes used in the half-gap experiments and was probably ad-

TABLE 2. Comparison of typical values of (left) the slope parameter s'/s and (right) the nondimensional current width for the gentle and steep slopes in the laboratory and in the WGC.

s'/s	Gentle	Steep
Laboratory	7–14	0–1
WGC	1–3	0.2–0.3
W/R_D	Gentle	Steep
Laboratory	10–30	0–7
WGC	10–40	4–16

equately modeled by the vertical wall (for which $s'/s = 0$) in the full-gap experiments. In contrast, the slope parameter over the gentle slope is much larger in the laboratory than in the WGC and, thus, the gentle slope was too gentle. Because the primary purpose of the gentle slope upstream of the gap in the full-gap experiments was simply to stabilize the current before it entered the gap, the exact value of the slope is not of great concern. However, application of the observation that the flow was immediately stabilized when inflowed from a steep slope to a gentle slope to the WGC might be suspect because the gentle slope is much more gentle than the analogous slope in the ocean.

The natural scale for length comparisons is the internal Rossby radius R_D. The mean Rossby radius in the Labrador Sea is $R_D \approx 5$–20 km [the low and high values are taken from Emery et al. (1984) and Spall and Pickart (2003), respectively]. Table 2 compares the nondimensional width W of the laboratory currents with the nondimensional width of the WGC [seaward of the shelf break, estimated from Cuny et al. (2002), their Fig. 8]. The laboratory currents can be seen to have approximately the appropriate width in comparison with their Rossby radii.

In section 4b, it was noted that the current width W must exceed the slope width L (i.e., we must have $W/L > 1$) before the current became unstable. The width of the Greenland continental slope can be measured directly from bathymetry maps and ranges from < 20 km in the gap (around 61°N, 50°W) to ~180 km upstream of the gap (around 59°N, 44°W). The stability parameter W/L can then be calculated directly; its value ranges from ~1 upstream of the gap where the WGC is stable to ~4 inside the gap where the WGC is unstable. Thus, the observed stability characteristics of the WGC are consistent with the criterion for instability ($W/L > 1$) established by the present experiments.

Note that in the above analysis, we are implicitly assuming the Labrador Sea is unstratified. This is a good assumption following winter convection, which leaves the Labrador Sea essentially homogeneous in comparison with its boundary currents. To apply the instability criterion to a more strongly stratified system, the definition of slope width L must be modified because strong stratification shields the surface and interior from the influence of the bathymetry. The appropriate definition for L is the distance from the shelf break to the point where the water becomes deep enough that the ambient stratification becomes important. The depth at which this occurs is approximately equal to the scale depth of the first baroclinic vertical mode.

Energy budget estimates by Eden and Böning (2002) suggest that the WGC becomes barotropically unstable inside the gap, while Katsman et al. (2004) conclude that the instability is mixed. Both studies find that the energy conversion rate is greatest immediately downstream of the beginning of the slope change, although growing instabilities are not visible until several hundred kilometers downstream. It was not practical to determine the instability type or to measure the spatial distribution of energy conversion to instabilities in the laboratory experiments, though the similarity of the instabilities observed here and those observed in previous studies (Cenedese and Linden 2002) strongly suggests that the instabilities have a significant baroclinic component. Further, the fact that instabilities simultaneously appeared along the length of the steep slope in the half-gap experiments implies that there was no distinct maximum in energy conversion near the beginning of the steep slope. The exception was the experiments where the steep slope was replaced by a vertical wall, in which case an eddy began forming as soon as the current flowed onto the vertical wall.

The maximum eddy variability in the Labrador Sea is found at the downstream end of the gap, near where the 3000-m isobath diverges from the coast (Prater 2002; Lilly et al. 2003). The WGC bifurcates here, with the nearshore portion of the current system remaining attached to the coast and the offshore portion following the 3000-m isobath around the northern boundary of the Labrador Sea (Cuny et al. 2002). In the present study, eddies formed in the gap are advected downstream by the mean flow and accumulate at the downstream end of the gap because they are unable to propagate onto the gentle bathymetry. In the Labrador Sea, the eddies are able to eventually escape along the 3000-m isobath (Prater 2002), while, in these experiments, they are simply displaced offshore by new eddies formed inshore.

The numerical experiments of Katsman et al. (2004) demonstrate that the bathymetric constriction must exceed a certain downstream length scale before eddies would form in the gap. If the gap had a length of 200 km (10–$40R_D$), the current would meander as soon as it entered the gap, but be stabilized as it flowed onto the gentle bathymetry downstream of the gap. When the gap length was increased to 400 km (20–$80R_D$), eddies with characteristics similar to the observed WGC eddies began to form. This is qualitatively similar to the behavior observed in the full-gap experiments where the gap had to exceed a critical length that was between $16R_D$ and $32R_D$ before eddies could be formed continuously in the gap. It is difficult to make the comparison more precise because estimates of the Rossby radius in the Labrador Sea can vary by as much as a factor

of 4. In addition, the true Rossby radius in the experiments may be reduced by as much as 15% because of the modification of the reduced gravity g' by mixing.

The scale of the eddies themselves, on the other hand, compares quite favorably. An extensive survey of eddies in the Labrador Sea by Lilly et al. (2003) found that WGC eddies have radii of 15–30 km (1–6R_D). Katsman et al.'s (2004) numerical model produced eddies with very similar characteristics; they had a core of buoyant water and an average radius of approximately 25 km (1–5R_D) The eddies observed in the present experiments had radii of 4–5 cm (3–4R_D), which is quite similar to that of the Irminger rings.

Note that in the present experiments, the β effect is absent. Given the smallness of the scales of motion relative to planetary scales and the strength of the bottom slope, the β effect is not expected to play a large role in determining the rate of eddy formation. Once formed, the β effect would cause the eddies to drift westward out of the gap with speed $c \approx \beta R_d^2$ (see, e.g., Cushman-Roisin et al. 1990 and the references therein). For the region under consideration, this speed is so slow that the eddies are expected to drift less than 10 km in the time it takes them to transit the gap, reaffirming the fact that the β effect is negligible in this system.

8. Summary

The objective of this paper was to examine how changing bathymetry controls the stability of a buoyant coastal current, with a specific focus on the generation of eddies in the Labrador Sea as the WGC flows through a bathymetric constriction in the continental slope (i.e., the gap with a very steep slope). It was hypothesized that rapid downstream changes in the bathymetric slope could induce instability and eddy formation. Two sets of laboratory experiments were performed to test this hypothesis. The first set, the half-gap experiments, focused on the dynamics of the extreme upstream or downstream end of the bathymetric constriction to determine if a buoyant coastal current flowing from a gentle slope to a steep slope could trigger eddy formation and if these eddies, once formed, could move onto a gentle slope. The second set, the full-gap experiments, examined the effect of varying the downstream length scale of the bathymetric constriction containing a destabilizing slope. It was expected that a sufficiently small gap would be traversed by a current without the occurrence of instability.

It was found that the sloping bathymetry exerts a stabilizing influence so strong that the current was always stable as long as it was less wide than the sloping bathymetry, regardless of the upstream conditions. Once the current was wider than the bathymetry, it became rapidly unstable and formed eddies. These eddies formed nearly simultaneously along the edge of the front and did not appear to be influenced by the abruptness of the transitions between the different slopes. The extreme case of a buoyant current flowing from a gentle slope onto a vertical wall was exceptional, because the current was always wider than the bathymetry. In this case, an eddy formed within about 25 cm (20 Rossby radii) of the beginning of the vertical wall.

The full-gap experiments fell into three regimes depending on the downstream length of the gap. For gaps smaller than $8R_D$ (the length scale of the initial instabilities), no eddies formed in the gap, while eddies would form continuously for gaps $\gtrsim 32R_D$. These two regimes were separated by an intermediate regime where the eddy field would saturate with only a few eddies that would remain trapped in the gap.

The cross- and along-stream length conditions for instability ($W/L > 1$ and $a \gtrsim 32R_D$, respectively) deduced from the laboratory experiments are consistent with observations and numerical simulations of the WGC. In addition, the scales of the currents and eddies produced in the experiments are very similar to those observed in the Labrador Sea. These results add weight to the hypothesis that Irminger ring formation is triggered by the narrow, steep continental slope west of Greenland and, additionally, suggest that the WGC becomes unstable because the slope is sufficiently narrow that the outcrop of the current is no longer constrained by the slope.

Acknowledgments. The authors gratefully acknowledge the National Science Foundation (Grant OCE-9810657) and the Office of Naval Research (Grant N00014-97-1-0934) for their support of the 2003 WHOI Geophysical Fluid Dynamics Summer School where much of the research presented in this paper was performed. CLW received additional support from the Office of Naval Research Grant N00014-98-1-0813. We thank K. Bradley for providing invaluable assistance in the lab. Thanks are also given to R. Pickart, R. Samelson, and M. Spall for their helpful comments on the manuscript. CLW is especially grateful to his advisor R. Samelson for giving him leave to work on this project.

REFERENCES

Blumsack, S. L., and P. J. Gierasch, 1972: Mars: The effects of topography on baroclinic instability. *J. Atmos. Sci.,* **29,** 1081–1089.

Bracco, A., and J. Pedlosky, 2003: Vortex generation by topography in locally unstable baroclinic flows. *J. Phys. Oceanogr.,* **33,** 207–219.

Cenedese, C., and P. F. Linden, 2002: Stability of a buoyancy-driven coastal current at the shelf break. *J. Fluid Mech.,* **452,** 97–121.

Chapman, D. C., and S. J. Lentz, 1994: Trapping of a coastal density front by the bottom boundary layer. *J. Phys. Oceanogr.,* **24,** 1464–1479.

Condie, S. A., 1993: Formation and stability of shelf break fronts. *J. Geophys. Res.,* **98,** 12 405–12 416.

Cuny, J., P. B. Rhines, P. P. Niiler, and S. Bacon, 2002: Labrador Sea boundary currents and the fate of the Irminger Sea Water. *J. Phys. Oceanogr.,* **32,** 627–647.

Cushman-Roisin, B., E. P. Chassignet, and B. Tang, 1990: Westward motion of mesoscale eddies. *J. Phys. Oceanogr.,* **20,** 758–768.

Eden, C., and C. Böning, 2002: Sources of eddy kinetic energy in the Labrador Sea. *J. Phys. Oceanogr.,* **32,** 3346–3363.

Emery, W. J., W. G. Lee, and L. Magaard, 1984: Geographic and seasonal distributions of Brunt-Väisälä frequency and Rossby radii in the North Pacific and North Atlantic. *J. Phys. Oceanogr.,* **14,** 294–317.

Flagg, C. N., and R. C. Beardsley, 1978: On the stability of the shelf water/slope water front south of New England. *J. Geophys. Res.,* **83,** 4623–4631.

Gawarkiewicz, G., 1991: Linear stability models of shelfbreak fronts. *J. Phys. Oceanogr.,* **21,** 471–488.

Gill, A. E., J. S. A. Green, and A. J. Simmons, 1974: Energy partition in the large-scale ocean circulation and the production of mid-ocean eddies. *Deep-Sea Res.,* **21,** 499–528.

Hide, R., A. Ibbetson, and M. J. Lighthill, 1968: On slow transverse flow past obstacles in a rapidly rotating fluid. *J. Fluid Mech.,* **32,** 251–272.

Katsman, C. A., M. A. Spall, and R. S. Pickart, 2004: Boundary current eddies and their role in the restratification of the Labrador Sea. *J. Phys. Oceanogr.,* **34,** 1967–1983.

Krauss, W., 1986: The North Atlantic Current. *J. Geophys. Res.,* **91,** 5061–5074.

——, 1995: Currents and mixing in the Irminger Sea and in the Iceland Basin. *J. Geophys. Res.,* **100,** 10 851–10 871.

Lentz, S., and K. Helfrich, 2002: Buoyant gravity currents along a sloping bottom in a rotating fluid. *J. Fluid Mech.,* **464,** 251–278.

Lilly, J. M., P. B. Rhines, F. Schott, K. Lavender, J. Lazier, U. Send, and E. D'Asaro, 2003: Observations of the Labrador Sea eddy field. *Progress in Oceanography*, Vol. 59, Pergamon, 75–176.

Orlanski, I., 1968: The instability of frontal waves. *J. Atmos. Sci.,* **25,** 178–200.

Pedlosky, J., 1964: The stability of currents in the atmosphere and ocean, I. *J. Atmos. Sci.,* **21,** 201–219.

Pickart, R. S., D. J. Torres, and R. A. Clark, 2002: Hydrography of the Labrador Sea during active convection. *J. Phys. Oceanogr.,* **32,** 428–457.

——, ——, and P. S. Fratantoni, 2005: The east Greenland spill jet. *J. Phys. Oceanogr.,* **35,** 1037–1053.

Prater, M. D., 2002: Eddies in the Labrador Sea as observed by profiling RAFOS floats and remote sensing. *J. Phys. Oceanogr.,* **32,** 411–427.

Samelson, R. M., and J. Pedlosky, 1990: Local baroclinic instability of flow over variable topography. *J. Fluid Mech.,* **221,** 411–436.

Spall, M. A., 2004: Boundary currents and watermass transformation in marginal seas. *J. Phys. Oceanogr.,* **34,** 1197–1213.

——, and R. S. Pickart, 2003: Wind-driven recirculations and exchange in the Labrador and Irminger Seas. *J. Phys. Oceanogr.,* **33,** 1829–1845.

Sverdrup, H. U., M. W. Johnson, and R. H. Fleming, 1942: *The Oceans: Their Physics, Chemistry, and General Biology.* Prentice Hall, 1087 pp.

Yankovsky, A. E., and D. C. Chapman, 1997: A simple theory for the fate of buoyant coastal discharges. *J. Phys. Oceanogr.,* **27,** 1386–1401.